Available online at www.sciencedirect.com
SCIENCE DIRECT
Engineering Structures 28 (2006) 1715–1727
ENGINEERING STRUCTURES
www.elsevier.com/locate/engstruct

Implementation of bond-slip effect in analyses of RC frames under cyclic loads using layered section method

Hyo-Gyoung Kwak*, Jin-Kook Kim

Department of Civil and Environmental Engineering, Korea Advanced Institute of Science and Technology, 373-1 Guseong-dong, Yuseong-gu, Daejeon 305-701, Republic of Korea

Received 5 March 2005; received in revised form 24 February 2006; accepted 6 March 2006
Available online 24 April 2006

Abstract

A nonlinear dynamic finite element analysis of reinforced concrete (RC) frames subject to both dynamic and cyclic loadings is performed using the layered section method. In contrast to conventional layered section approaches that adopt a perfect bond assumption, the bond-slip effect along the reinforcing bar is quantified with the force equilibrium and compatibility condition at the post-cracking stage and its contribution is indirectly implemented into the stress–strain relation of reinforcing steel. Thus, the advantage of the proposed analytical procedure is that it takes the bond-slip effect into account while using the conventional layered section method, without the need for additional considerations such as taking the double nodes. Comparisons between experimental data and analytical results verify that the proposed analytical procedure can effectively simulate the cracking behavior of RC beams, columns, and frames that accompanies the stiffness degradation caused by bond-slip.

Keywords: Layered section model; Bond-slip; Transfer length; Cyclic loading; RC frame

1. Introduction

The ultimate design objective for structural engineers is the creation of safe and economical structures. To this end, advanced analytical tools can be indispensable aids for assessing the safety and serviceability of a proposed design. Such assessments are especially important for complex modern structures such as nuclear power plants, long-span bridges, and high-rise buildings, which are subjected to very complex load histories. Time-consuming and costly, experimental studies actually produce very limited data in terms of structural responses. Therefore, in order to perform safety and serviceability assessments of complex structures, it is necessary to develop reliable numerical methods and models. Accordingly, many numerical studies have been performed [1–4]. In relation to this, enhanced building and bridge design codes for RC (reinforced concrete) structures subject to ultimate loads have accelerated the development of numerical models that can effectively simulate the nonlinear dynamic behavior of RC structural members.

In order to ensure that serviceability requirements are met in an RC structure, it is necessary to predict the cracking and the deflection of the structure under service loads. Therefore, estimation of the ultimate load is essential in assessing the margin of safety of RC structures against failure. Furthermore, it is necessary to predict the load–deformation behavior of the structure for responses ranging from elastic to inelastic as well as under all possible loading conditions, including monotonic, cyclic, and dynamic loading. RC frame structures in regions of high seismic risk particularly tend to develop inelastic deformations when subjected to strong earthquakes. Accordingly, a complete assessment of the seismic resistant design of RC frame structures often requires a nonlinear dynamic analysis. The nonlinear dynamic responses of RC frame structures under earthquake excitations are usually developed at certain critical regions, which are often located at points of maximum internal forces, such as at the beam–column joints. Thus, a reliable numerical model that can simulate the hysteretic behavior of RC columns and beams is necessary for predicting the nonlinear response of the frame structures. Since

* Corresponding author. Tel.: +82 42 869 3621; fax: +82 42 869 3610.
E-mail addresses: khg@kaist.ac.kr (H.-G. Kwak), glory95@kaist.ac.kr (J.-K. Kim).

0141-0296/$ - see front matter © 2006 Elsevier Ltd. All rights reserved.
doi:10.1016/j.engstruct.2006.03.003

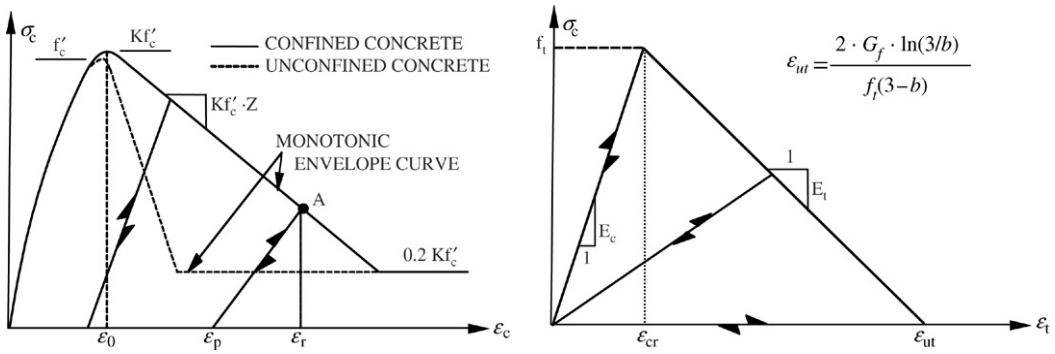

(a) Compressive region. (b) Tensile region [15].

Fig. 1. Stress–strain relation of concrete.

earthquake-induced energy is dissipated through the formation of plastic hinges in the beams and columns, determining the influencing factors that affect the nonlinear response at a joint is essential in the construction of a numerical model. Initial stiffness, bond-slip, anchorage slip, shear span ratio, and axial force effects are some of the typical influencing factors that must be included in the numerical model, as major sources of deformation in RC frame structures are flexural rotation and bond-slip. The hysteretic load–deformation behavior of a frame member results from a combination of these deformation mechanisms.

To date, many analytical models have been proposed for the nonlinear analysis of RC frame structures; these range from very refined and complex local models to simplified global models [5,6]. In the case of frame structures, a numerical model based on the moment–curvature relation is often used. Since the bilinear moment–curvature relationship by Clough and Johnson [7] was first introduced, many mechanical models for the hysteretic moment–curvature relationship have been proposed to analyze the behavior of RC beams subjected to cyclic loading. These models include cyclic stiffness degradation [4,8,9]. Further modifications have also been introduced to consider the pinching effects due to shear force and strength degradation after yielding of steel [2]. Recently, many researchers have focused on including axial load and bond-slip effects in their models [2,10,11]. Nevertheless, all of these models based on the moment–curvature relation are still limited in terms of simulating exact structural behavior, because they exclude the internal force variation according to the loading history.

In this paper, a new numerical model based on the layer approach is introduced. The constitutive relation of an RC section is not specified explicitly in this model. Instead, it is derived by integration of the response of the imaginary layers, which follows the uniaxial stress–strain relation of the particular material. Therefore, changes in internal member forces, such as the biaxial bending moments and the axial force, can effectively be implemented through the force equilibrium in a section. However, the conventional layer models have a fundamental limitation in that they ignore the bond-slip effect [12]. In order to overcome this shortcoming, the numerical model introduced in this paper considers the bond-slip effect by defining a modified initial loading branch on the basis of the monotonic stress–strain relation of the reinforcing steel. The validity of the proposed model is established by comparing analytical predictions with results from experimental studies. The results of a correlation study based on the analytical results and experimental values from an RC frame structure subject to an earthquake loading testify to the applicability of the introduced model to the nonlinear dynamic analysis of RC frame structures.

2. Stress–strain relation of concrete

2.1. Monotonic envelope curve

The response of RC members under loads depends to a large extent on the stress–strain relation of the constituent materials and on the magnitude of the stress. Since concrete is used mostly in compression, the stress–strain relation in compression is of primary interest. Among the numerous mathematical models currently used in the analysis of RC structures, the monotonic envelope curve for the concrete confined by rectangular hoops introduced by Kent and Park [13] and later extended by Scott et al. [14] is adopted in this paper because of its simplicity and computational efficiency. In this model, as shown in Fig. 1(a), the monotonic concrete stress–strain relation in compression has three discrete regions:

$$\sigma_c = K f_c' \left[2\left(\frac{\varepsilon_c}{\varepsilon_0}\right) - \left(\frac{\varepsilon_c}{\varepsilon_0}\right)^2 \right], \quad \varepsilon_c \le \varepsilon_0 \tag{1}$$

$$\sigma_c = K f_c' \left[1 - Z\left(\varepsilon_c - \varepsilon_0\right)\right], \quad \varepsilon_0 \le \varepsilon_c \le \varepsilon_u \tag{2}$$

$$\sigma_c = 0.2 K f_c', \quad \varepsilon_c \ge \varepsilon_u \tag{3}$$

where

$$\varepsilon_0 = 0.002K, \quad K = 1 + \frac{\rho_s f_{yh}}{f_c'}, \quad \varepsilon_u = \varepsilon_0 + 0.8/Z \tag{4}$$

$$Z = \frac{0.5}{\frac{3+0.290 f_c'}{144.0 f_c' - 1000} + 0.75\rho_s\sqrt{\frac{h'}{s_h}} - 0.002K} \tag{5}$$

where ε_o is the concrete strain at maximum stress, K is a factor that accounts for the strength increase due to confinement, Z is the strain softening slope, f_c' is the concrete compressive strength in MPa, f_{yh} is the yield strength of the stirrups in

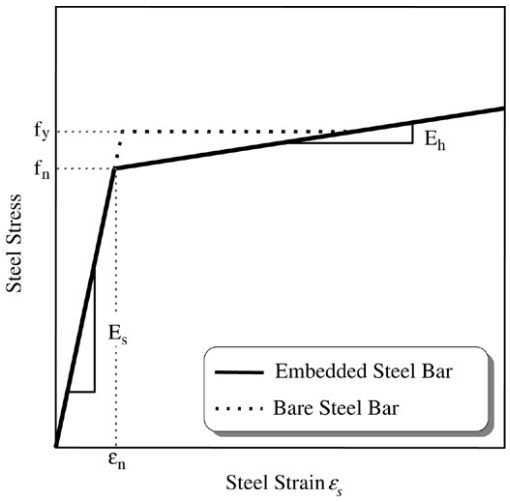

Fig. 2. Stress–strain relation of steel (Belarbi and Hsu [22]).

MPa, ρ_s is the ratio of the volume of hoop reinforcement to the volume of concrete core measured to the outside of the stirrups, h' is the width of the concrete core measured to the outside of the hoops or ties, and s_h is the center to center spacing of tie or hoop sets. In Eq. (5), the first term of the denominator, $(3 + 0.290 f_c')/(144.0 f_c' - 1000)$, takes into account the effect of concrete strength on the slope of the falling branch of unconfined concrete, and the second term of the denominator, $0.75\rho_s\sqrt{h'/s_h}$, considers the additional ductility developed by lateral confinement with rectangular hoops.

On the other hand, it is assumed that concrete is linearly elastic in the tension region. Beyond the tensile strength, the tensile stress decreases linearly with increasing principal tensile strain (see Fig. 1(b)). Ultimate failure from cracking is assumed to occur when the principal tensile strain exceeds the value $\varepsilon_{ut} = 2 \cdot G_f/f_t' \cdot \ln(3/b)/(3 - b)$ in Fig. 1(b), where b denotes the element length used in the finite element analysis and G_f is the fracture energy that is dissipated in the formation of a crack of unit length per unit thickness and is considered a material property. The value of ε_{ut} is derived from the fracture mechanics concept by equating the crack energy release with the fracture toughness of concrete G_f [15]. An experimental study by Welch and Haismen [16] indicates that for normal strength concrete the value of G_f/f_t' is in the range of 0.005–0.01 mm. If G_f and f_t' are known from measurements, then ε_{ut} can be determined.

2.2. Definition of hysteretic behavior

After defining the monotonic envelope curves, the unloading –reloading branches need to be defined in order to simulate the hysteretic behavior of concrete. Since a cyclic stress–strain curve describes the changing material properties of concrete under cyclic loadings, its exact definition is first required. However, unlike the envelope curves obtained from monotonic loading tests, the difficulties involved in conducting experiments for plain concrete subject to cyclic loadings make it almost impossible to develop a mathematical model of a cyclic stress–strain curve based on experimental results. For this reason, related research has been limited [17,18], and only a few cyclic stress–strain curves have been introduced through experimental studies [18,19].

The unloading–reloading behavior of cracked concrete is particularly complex, and the cyclic behavior of concrete is generally defined by the unloading–reloading curves that connect several key points: the maximum strain, the common point, the permanent strain, and the restoring strain. Accordingly, to define the cyclic behavior of concrete, simplified unloading–reloading curves are generally adopted for their simplicity and computational efficiency in providing numerical analyses of RC structures [20]. However, the use of a simplified relation must be limited to the case of bending members and/or axial members such as RC beams and/or slabs, because the main part of these structures experiences a biaxial stress combination in the tension–tension or compression–compression region of the biaxial strength envelope.

It is assumed that the following rules given in Eqs. (6) and (7) govern the hysteretic behavior of the concrete stress–strain relation in the compression region (see Fig. 1(a)). In addition, the unloading–reloading branches that always pass the origin regardless of the loading history are assumed in the tension region (see Fig. 1(b)), because application of the introduced numerical model is limited to RC frame structures [5,20]. Eqs. (6) and (7) were proposed by Karsan and Jirsa [19] and define a straight line connecting the point ε_r in Fig. 1(a) where unloading starts to a point ε_p on the strain axis.

$$\frac{\varepsilon_p}{\varepsilon_0} = 0.145 \cdot \left(\frac{\varepsilon_r}{\varepsilon_0}\right)^2 + 0.127 \cdot \left(\frac{\varepsilon_r}{\varepsilon_0}\right), \quad \left(\frac{\varepsilon_r}{\varepsilon_0}\right) < 2 \tag{6}$$

$$\frac{\varepsilon_p}{\varepsilon_0} = 0.707 \cdot \left(\frac{\varepsilon_r}{\varepsilon_0} - 2\right) + 0.834, \quad \left(\frac{\varepsilon_r}{\varepsilon_0}\right) \geq 2. \tag{7}$$

3. A proposed stress–strain relation of steel

3.1. Reduction of yielding stress

Reinforcing steel is usually modeled as a linear elastic, linear strain hardening material with a yield stress f_y. However, when reinforcing bars are surrounded by concrete, the average behavior of the stress–strain relation is quite different, as shown in Fig. 2 [22]. The most strikingly different feature is the lowering of the yield stress below f_y. Yielding of an RC member occurs when the steel stress at a cracked section reaches the yield strength of the bare bar. However, the average steel stress at a cracked element still maintains an elastic stress that is less than the yield strength, because the concrete matrix located between cracks is still partially capable of resisting tensile forces, owing to the bond between the concrete and the reinforcement. Determination of element stiffness on the basis of the yielding of steel at a cracked section where a local stress concentration appears in the steel may result in overestimation of the structural response at the post-yielding range. Since this phenomenon is accelerated with increased deformation, an analysis of RC members subject to cyclic

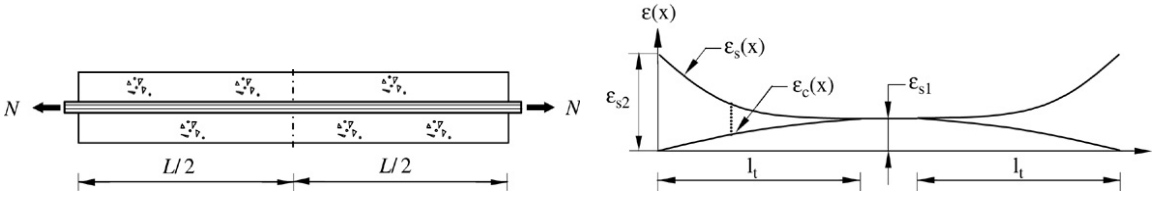

(a) Tension member. (b) Strain distribution.

Fig. 3. Behavior of tension member.

loading accompanying relatively large deformations requires the use of average stress–strain relations [21,22].

Accordingly, the average stress–strain relation of steel needs to be defined so as to trace the cracking behavior of RC beams and/or columns up to the ultimate limit state. This can be accomplished by using the smeared crack model, in which the local displacement discontinuities at cracks are distributed over some tributary area within the finite element and where the behavior of cracked concrete is represented by the average stress–strain relations [21]. Considering these factors, the following linear average stress–strain relation, which was introduced by Belarbi and Hsu [22] from experimental data, is used in this paper to revise the monotonic envelope curve of steel.

$$\sigma_s = E_s \cdot \varepsilon_s, \quad \varepsilon_s \le \varepsilon_n \tag{8}$$

$$\sigma_s = f_n + (0.02 + 0.25B)\, E_s(\varepsilon_s - \varepsilon_n), \quad \varepsilon_s \ge \varepsilon_n \tag{9}$$

where σ_s and ε_s represent the average strain and stress, respectively, and f_y and ε_y are the yield stress and the corresponding yield strain of a bare steel bar, respectively. As shown in Eq. (9), the average stress σ_s is a linear function of the parameter $B = (f_t'/f_y)^{1.5}/\rho$ and is limited by the boundary strain $\varepsilon_n = \varepsilon_y(0.93 - 2B)$ for the yielding of steel, where ρ is the percentage of the steel ratio and must be greater than 0.5%. More details on the average stress–strain relation of steel can be found elsewhere [22].

3.2. Bond-slip effect on stress–strain relation

Reinforcing bars transfer tensile stresses to concrete through the bond stresses located along the surface between reinforcements and surrounding concrete. In this way, part of an RC member subjected to uniaxial tension and bounded by two adjacent cracks can be extracted and used as a free body diagram to obtain the equilibrium equations for concrete and steel (see Fig. 3(a)). When the axial load N is applied, the far ends represent the fully cracked state with a steel strain of ε_{s2} (see Fig. 3(b)). For this application, the tensile force N is first transferred from the steel bar to the concrete by bond stress, and the value of the bond stress is zero at the inner part $(L - 2l_t)$. This means that there is no bond-slip within the central region bounded by the transfer length. Moreover, it can be assumed that the strains in steel and concrete are equal to each other at $x = l_t$ and that the strain value corresponds to ε_{s1} (see Fig. 3(b)).

From the strain distribution, the local slip $s(x)$ can be defined as the total difference in elongations between the reinforcement and the concrete matrix measured over the length between a distance x from a crack face and the center of the segment $(x = L/2)$. That is,

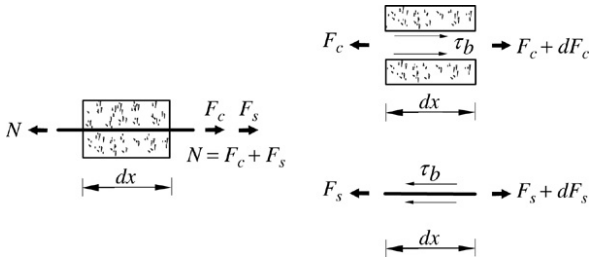

Fig. 4. Free body diagram for an RC member.

$$s(x) = \int_x^{L/2} (\varepsilon_s(x) - \varepsilon_c(x))\, \mathrm{d}x \tag{10}$$

where L is the length between two adjacent cracks, which is equivalent to the crack spacing, and $\varepsilon_s(x)$ and $\varepsilon_c(x)$ are the strain distributions of steel and concrete, respectively.

Since the applied tensile force of an RC member (N) is carried partly by the concrete matrix (F_c) and partly by the reinforcing steel (F_s), the force equilibrium of $N = F_c + F_s$ can be defined. First, as shown in Fig. 4's representation of the free body diagram of an axial member, the steel and concrete force variations can be derived in terms of the bond stresses.

$$\begin{aligned} \frac{\mathrm{d}F_s}{\mathrm{d}x} &= A_s E_s \frac{\mathrm{d}\varepsilon_s}{\mathrm{d}x} = m\Sigma_0\tau_b, \\ \frac{\mathrm{d}F_c}{\mathrm{d}x} &= A_c E_c \frac{\mathrm{d}\varepsilon_c}{\mathrm{d}x} = -m\Sigma_0\tau_b \end{aligned} \tag{11}$$

where m is the number of bars placed within an infinitesimal length $\mathrm{d}x$, Σ_0 is the perimeter of a reinforcing bar, τ_b is the bond stress at the steel concrete interface, and A and E are the corresponding cross-section area and the elastic modulus of each material, respectively.

On the basis of the bond-slip $s(x)$, as defined by the relative displacement between the reinforcing steel and the concrete (see Eq. (10)), the second order differential equation of the bond-slip leads to $\mathrm{d}^2s/\mathrm{d}x^2 = -\mathrm{d}/\mathrm{d}x(\varepsilon_s(x) - \varepsilon_c(x))$. After substituting Eq. (11) into this relation, and assuming the linear bond stress–slip relationship of $\tau_b = E_b \cdot s(x)$, the following governing differential equation is obtained:

$$\frac{\mathrm{d}^2 s}{\mathrm{d}x^2} - k^2 s = 0 \tag{12}$$

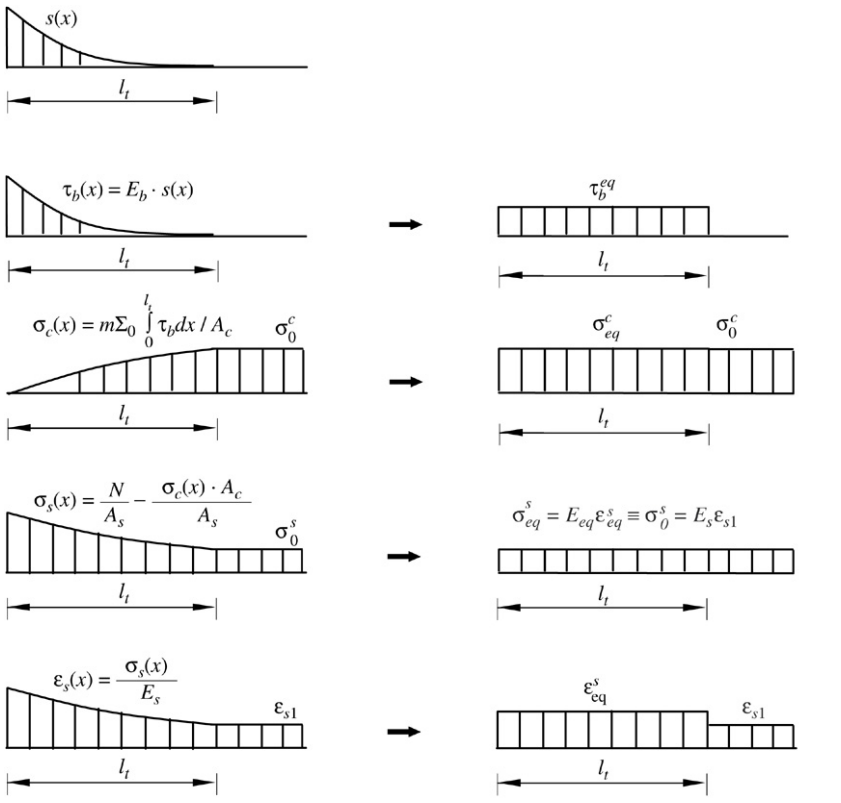

(a) Calculated distribution. (b) Transformed equivalent distribution.

Fig. 5. Distribution of slip and stresses between two adjacent cracks.

where $k^2 = m\Sigma_0 E_b(1 + n\rho)/A_s E_s$, $n = E_s/E_c$, $\rho = A_s/A_c$, and E_b is the slip modulus and is assumed to be 1.826 $\times 10^4$ MN/m^3.

The general solution to Eq. (12) is given by $s(x) = C_1 \sinh kx + C_2 \cosh kx$, in which C_1 and C_2 are constants that have to be determined from the two boundary conditions. That is, the slip should be zero at $x = l_t$ in Fig. 3 and has a maximum value of s_0 at $x = 0$, which is the crack face. Since it can be assumed that the crack width ω is equivalent to twice the bond-slip s_0 at the cracked location, the bond-slip s_0 can be expressed in terms of the corresponding crack width, $s_0 = \omega/2$. Since the small area around the reinforcing steel at the flexural crack surface of a reinforced concrete beam is similar to the end face of the tension member in Fig. 3(a), the solution of Eq. (12) may be applied to bending members. A relation introduced by Gergely and Lutz [23], which is commonly used to determine the allowable crack width of cracked RC frame members, is adopted in this paper.

$$\omega_{\max} = 1.08\beta_c f_s \sqrt[3]{d_c A} \times 10^{-5}\,\text{mm} \tag{13}$$

where β_c is the ratio of distances from the tension face and from the steel centroid to the neutral axis and d_c is the thickness of the concrete cover. A is equal to A_e/m, the effective tension area of concrete surrounding the main tension reinforcing bars, where m is the number of bars in tension and A_e is $2d_s * b_0$, where d_s is the distance to the centroid of the tension bar group and b_0 is the width of a section. Moreover, the transfer length l_t can be determined either from the force equilibrium of $N = \varepsilon_{s2} \cdot A_s E_s = \varepsilon_{s1}(A_s E_s + A_c E_c) = F_c(1 + n\rho)$, as in Fig. 3, and the relation of Eq. (14)

$$F_c|_{x=l_t} = \frac{N}{1+n\rho} = -m\Sigma_0 \int_0^{l_t} \tau_b(s)\mathrm{d}x = -m\Sigma_0 E_b \int_0^{l_t} s(x)\mathrm{d}x \tag{14}$$

or by the following linear relationship proposed by Somayaji and Shah [24] on the basis of much experimental data from pull-out tests:

$$l_t = K_p \cdot \frac{F_c}{\Sigma_0} \tag{15}$$

where F_c is the transfer load equal to $F_c = A_c E_c \varepsilon_{s1} = N/(1 + n\rho)$, and K_p is a constant determined from the pull-out test. An experimental study by Mirza and Houde [25] indicates that the value of K_p is in the range of 2.028–5.441 1/MPa. Therefore, the average value of 3.76 1/MPa is used in this paper.

Determination of the bond characteristics along the member makes it possible to obtain the unique distribution of slip and stresses between two adjacent cracks, as shown in Fig. 5(a). First, for the applied axial force N, the load carried by the concrete and by the steel can be defined by $F_c = \sigma_c(x)A_c$ and $F_s = \sigma_s(x)A_s = N - F_c$, respectively. Accordingly, using the relation between the bond stress and the force component in

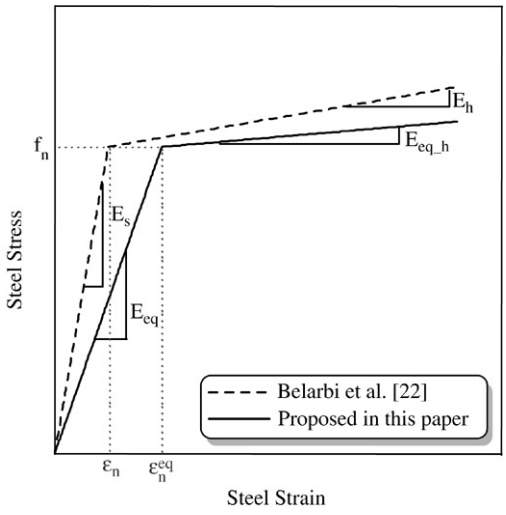

Fig. 6. Equivalent stress–strain relation of steel.

Eq. (11), the steel stress can be expressed by

$$\sigma_s(x) = \frac{N}{A_s} - \frac{\sigma_c(x)A_c}{A_s} = \frac{N}{A_s} + \frac{m\Sigma_0\tau_b^{eq}}{A_s}x \tag{16}$$

where $\tau_b^{eq} = \int_0^{l_t} \tau_b(s)\mathrm{d}x/l_t$ is the equivalent average bond stress introduced in this paper for computational convenience (see Fig. 5(b)). In Fig. 5(b), the average steel strain ε_{eq}^s can also be calculated by $\varepsilon_{eq}^s = \int_0^{l_t} \varepsilon_s(x)\,\mathrm{d}x/l_t$.

Since the layer model basically adopts the perfect bond assumption, the steel stress must maintain a constant value along the element length unless the magnitude of the applied axial load is not changed. This means that the equivalent steel stress within the transfer length must be the same as the steel stress outside of this range. That is, $\sigma_{eq}^s = E_{eq}\varepsilon_{eq}^s \equiv \sigma_0^s = E_s\varepsilon_{s1}$ in Fig. 5 must be satisfied. Further, the corresponding equivalent modulus of elasticity for steel can finally be determined by $E_{eq} = E_s\varepsilon_{s1}/\varepsilon_{eq}^s$ up to the yielding point in the stress–strain relation of the embedded reinforcing steel, as depicted by the solid line in Fig. 2. The same ratio of E_{eq} to E_s is assumed to be maintained at the post-yielding region, and Fig. 6 shows the stress–strain relation of steel that is finally constructed by considering the bond-slip effect.

The stress–strain relation for compressive steel is defined by the same envelope curve as that used for tensile steel. This is because it is assumed, in the case of compressive steel, that the reduction of yield strength can be explained by the possibility of local buckling in the reinforcing steel embedded in the concrete matrix when it is subjected to a compressive axial force. Moreover, when subjected to a tensile axial force, the cyclic loading accompanying repeated crack opening and closing develops slip behavior even in compressive steel. Therefore, this paper uses the identical stress–strain relation defined in Fig. 6 to describe the nonlinear behavior of tensile and compressive steels.

3.3. Definition of hysteretic behavior

After modifying the monotonic envelope curve, it is then necessary to define the hysteretic curves. At load reversals, as shown in Fig. 7, the unloading stiffness is assumed to be the same as the initial stiffness. When loading continues in the opposite direction, the stress–strain curve exhibits the Bauschinger effect. This causes a nonlinear stress–strain relation and a reduction in stiffness of the stress–strain curve before the stress reaches the yield stress in the opposite direction. Among a number of models developed to describe the cyclic stress–strain curve of reinforcing steel [16], the most commonly used approach is the Giuffré–Menegotto–Pinto (G–M–P) model, introduced by Pinto et al. [26,27]; this model is also adopted in this paper. The stress–strain relation can be expressed by

$$\sigma^* = b\cdot\varepsilon^* + \frac{(1-b)\cdot\varepsilon^*}{\left(1+\varepsilon^{*R}\right)^{\frac{1}{R}}} \tag{17}$$

where $\varepsilon^* = (\varepsilon-\varepsilon_r)/(\varepsilon_0-\varepsilon_r)$, $\sigma^* = (\sigma-\sigma_r)/(\sigma_0-\sigma_r)$. Eq. (17) represents a curved transition from a straight line with slope E_0 to another asymptote with slope E_1, as represented by lines (a) and (b) in Fig. 7. The parameter b is the strain-hardening ratio between E_0 and E_1, ε_0 and σ_0 are the coordinates for the point at which the asymptotes of the branch under consideration meet (point A in Fig. 7(a)), and ε_r and σ_r are the strain and stress, respectively, at the point where the last strain reversal with stress of equal sign took place (point B in Fig. 7(a)). ε_0, σ_0, ε_r, and σ_r are updated at each strain reversal. R is a parameter that controls the shape of the transition curve and allows the representation of the Bauschinger effect. The expression for R is

$$R = R_0 - \frac{a_1\cdot\xi}{a_2+\xi} \tag{18}$$

where R is a decreasing function of ξ, which is the strain difference between the current asymptote intersection point (point A in Fig. 7(b)) and the previous load reversal point with maximum or minimum strain, depending on whether the corresponding steel stress at reversal is positive or negative (point A in Fig. 7(b)). ξ is updated following a strain reversal because the asymptote intersection point or the previous load reversal point with maximum or minimum strain may change. R_0, a_1, and a_2 are experimentally determined parameters. In this paper, it is assumed that $R_0 = 20$, $a_1 = 18.5$, and $a_2 = 0.15$, as used by Filippou et al. [28].

The original G–M–P model provides a good representation of complete stress–strain cycles but is problematic in terms of representing the isotropic strain hardening effect in the case of partial loading. In an effort to improve the applicability of the original G–M–P model, Filippou et al. [28] proposed a set of rules to shift the asymptote representing the yielding of steel. By horizontally moving the asymptote by σ_{st} before the asymptote intersection point (ε_0, σ_0) is newly calculated, the isotropic hardening effect can be considered. The shifting stress σ_{st} is calculated from

$$\frac{\sigma_{st}}{f_y} = a_3\left(\frac{\varepsilon_{\max}}{\varepsilon_y} - a_4\right) \tag{19}$$

where $\varepsilon_{\max}$ is the absolute maximum strain at strain reversal, and ε_y and f_y represent the yielding strain and

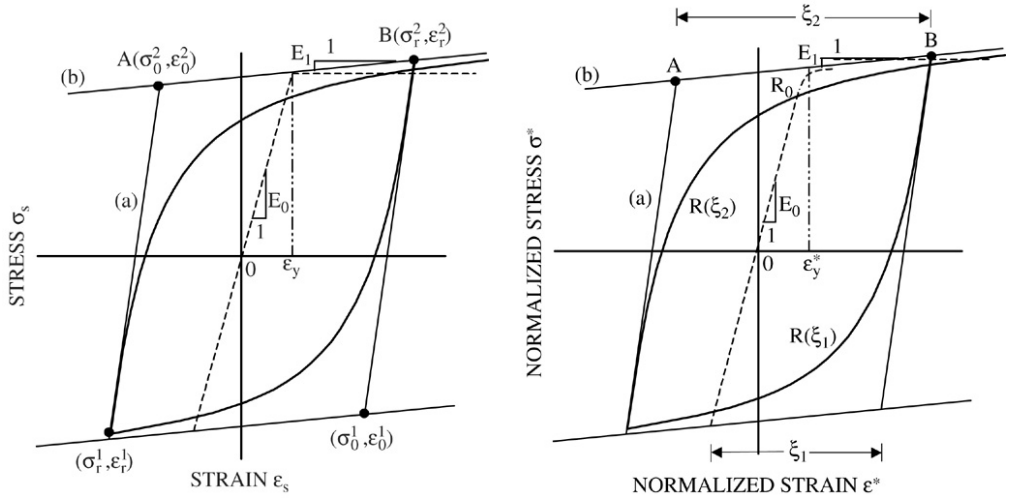

(a) Idealized representation. (b) Definition of curvature parameter R.

Fig. 7. A hysteretic stress–strain relation for steel.

stress, respectively. a_3 and a_4 are experimentally determined parameters; the values of $a_3 = 0.01$ and $a_4 = 7.0$ used by Filippou et al. [28] are assumed in this paper as well.

4. Solution algorithm

In order to analyze RC beams, a layer approach based on the Euler beam theory was used in this study. This approach and the beam theory are both well established and widely used in the analysis of beams, and as such more details for the formulation of beam elements can be found elsewhere [5,29]. In a typical Euler beam, it is usual to assume that plane sections remain plane to represent linearity in the strain distribution of any section at any loading history. In addition, the effects of shear deformation are not taken into consideration in simulating nonlinear behavior since the normal bending stresses reach a maximum at the extreme fibers, where the transverse shear stresses are at their lowest value, and reach a minimum where the transverse shear stresses are highest. Thus, the interaction between transverse shear stresses and normal bending stresses is relatively small and can be ignored. This means that the flexural rigidity EI is replaced by that corresponding to the curvature calculated from the nodal displacements. The shear rigidity of the beam element GA is assumed to be unchanged [11,13,30] and the shear modulus is calculated from $G = E/[2(1+\nu)]$.

Since the global stiffness matrix of the structure depends on the displacement increments, the solution of equilibrium equations is typically accomplished by an iterative method through a convergence check. The nonlinear solution scheme selected in this study uses a tangent stiffness matrix at the beginning of each load step in combination with a constant stiffness matrix during the subsequent correction phase; that is, an incremental-iterative method is used. All the remaining algorithms, from the construction of an element stiffness matrix to the iteration at each load step, are the same as those used in the conventional nonlinear analysis of RC structures; more details of these algorithms can be found elsewhere [5,12,15].

In this paper, only the dynamic equilibrium equation for a multi-degree of freedom system is briefly introduced. When a structure is subjected to ground acceleration, $\ddot{u}_g$, the incremental equation of the dynamic equilibrium can be written as

$$M\Delta\ddot{u} + C\Delta\dot{u} + K\Delta u = \Delta P = -M\{1\}\Delta\ddot{u}_g \tag{20}$$

where Δu, $\Delta\dot{u}$, and $\Delta\ddot{u}$ are the incremental displacement, velocity, and acceleration vectors during the time step Δt, respectively. M, C, and K are the mass, damping, and stiffness matrices, respectively. ΔP is the increment of external loads during the time step Δt and is given by $\Delta P = -M\{1\}\Delta\ddot{u}_g$, where $\{1\}$ is a unit vector. A lumped mass matrix M and Rayleigh damping matrix C are used in the analysis. The time history analysis of the structure is based on the average acceleration method, which is one of two special cases in Newmark's method because it does not require iteration to solve Eq. (20). More details can be found in Ref. [31].

5. Numerical analysis

5.1. RC beams subject to cyclic loadings

In order to establish the applicability of the modified stress–strain model of steel, two RC beams are investigated and discussed. These beams are specimen 40.048 (COLUMN1), experimented on by Wight and Sozen [32], and specimen 1 (COLUMN2), experimented on by Low and Moehle [30]. The material properties of each specimen are summarized in Table 1, where ρ_t and ρ_c are the steel ratios in the tension and compression parts, respectively.

The first specimen 40.048 consists of a reinforced concrete cantilever beam with a span length of 876 mm, and the transverse reinforcement is equally spaced at 88.9 mm. The beam was subjected to a cyclic lateral load V and a constant axial load P at the free end (see Fig. 8(a)). The plastic deformation is concentrated at the end of the beam with narrow width, accompanying the fixed-end rotation that occurs

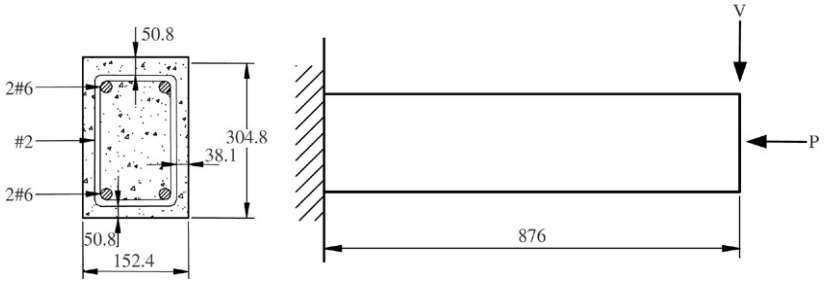

(a) COLUMN1.

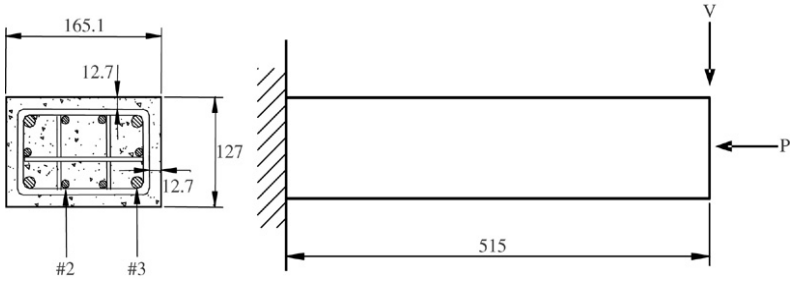

(b) COLUMN2.

Fig. 8. Details of specimens (unit: mm).

Table 1
Material properties used in application

Specimen	E_c (MPa)	E_s (MPa)	f'_c (MPa)	f_y (MPa)	$\rho_t = \rho_c$
COLUMN1	24,464	200,000	26	506	0.0122
COLUMN2	31,068	200,000	26	506	0.0113

Table 2
Transfer length and equivalent elastic modulus of steel E_{eq} for test specimens

Specimen	Transfer length (l_t: mm)	E_{eq} (MPa)
COLUMN1	658	118,588
COLUMN2	989	116,319

in addition to the elastic rotation at the large deformation stage. In order to more exactly simulate structural behavior that considers the beam element and is formulated on the basis of the average deformation in an element, separate consideration of this region is required in the finite element modeling. The plastic hinge length l_p is determined to be 200 mm according to a simple equation proposed by Sawyer [33]. Accordingly, the specimen is modeled along the entire span with an element of $l = 50$ mm.

In order to have moderate ductility, RC beams are generally designed to be subjected to less than about 10% of the axial strengths of their sections. Both specimens, COLUMN1 and COLUMN2, are loaded to 11% (equivalent to an axial force of 178.15 kN) and 4.5% (equivalent to an axial force of 44.54 kN) of their axial strengths, respectively. The transfer length calculated from Eq. (14) and the equivalent elastic modulus of steel determined on the basis of the proposed numerical model for COLUMN1 and COLUMN2 are listed in Table 2. When calculating those values, m of 2 and 4 and Σ_0 of 119.63 mm and 96.60 mm for COLUMN1 and COLUMN2, respectively, are used for calculation of the transfer length and the equivalent elastic modulus of steel.

This table shows that the transfer length in COLUMN2 is longer than the length of the specimen, which means that the equivalent elastic modulus of steel (E_{eq}) must be applied along the entire span because the bond-slip is expected to develop along the entire span.

As introduced by the load–deflection relations shown in Fig. 9, direct application of the elastic modulus of steel without additional considerations for the bond-slip between the reinforcing steel and its surrounding concrete matrix leads to hysteretic behavior with a high degree of error. When a shear dominant RC member, which is commonly thought to have a shear span ratio of less than 4.0, is subjected to cyclic loadings, it shows pinched hysteresis responses induced from the bond-slip at the anchorage region. In particular, if an RC member is axially loaded, even though it is not shear dominant, the axial force will cause the crack to open or close more rapidly to satisfy the force equilibrium of the section, and the resulting in a pinched hysteresis response. As seen in Fig. 8(a), COLUMN1 is a shear dominant RC member with a shear span ratio of 3.68 and is subjected to axial loading. Accordingly, the response obtained displays highly pinched behavior regardless of whether the equivalent elastic modulus for steel is considered, as shown in Fig. 9. Fig. 9 also shows that the basic layered section approach overestimates the energy absorption capacity of the beam—this is considered to be the most important factor affecting the serviceability of the structure. Meanwhile, the proposed model effectively estimates the energy absorption capacity and simulates the pinching phenomenon even at the large deformation stage.

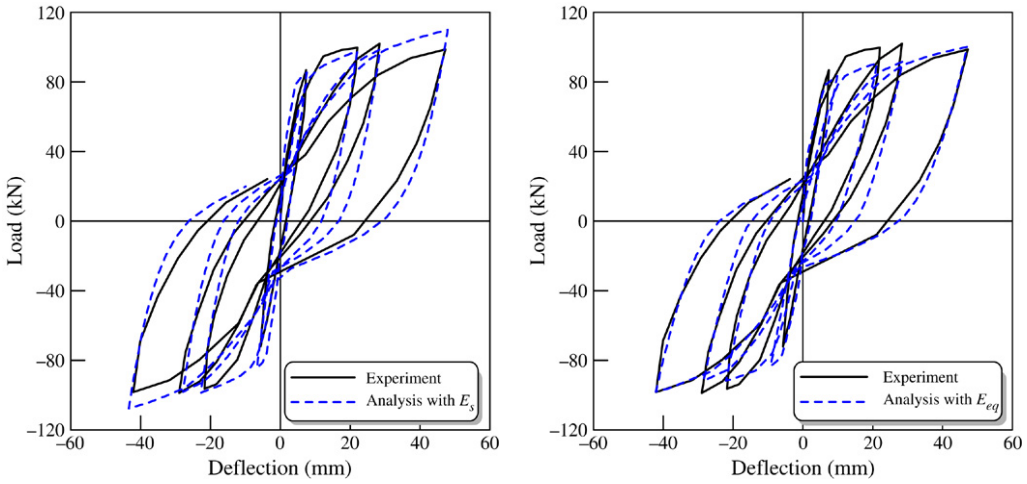

(a) Basic layered section model. (b) Proposed model.

Fig. 9. Load–deflection relation of COLUMN1.

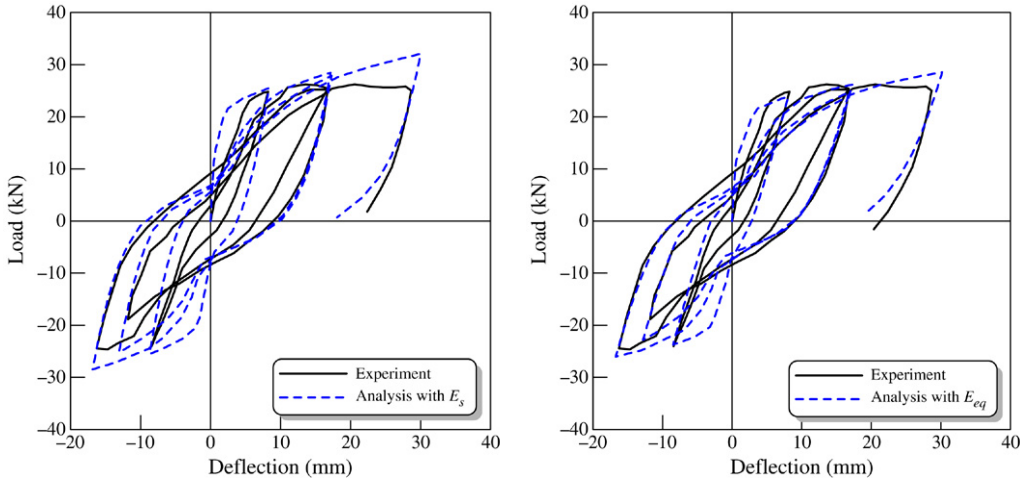

(a) Basic layered section model. (b) Proposed model.

Fig. 10. Load–deflection relation of COLUMN2.

The second specimen (COLUMN2) has a similar shape to the first specimen. No. 9 wire (7.935 mm^2) was used as transverse reinforcement in the columns. Starting from the left end of the column, the tie spacing was 25.4 mm for the first 228.6 mm followed by ties situated at every 38.1 mm on centers. The geometry and cross-section dimensions are presented in Fig. 8(b), and this example structure is modeled along the entire span with an element of $l = 40$ mm in consideration of the plastic hinge length.

As shown in Fig. 10, COLUMN2 shows lower pinched behavior than COLUMN1. This is because the shear span ratio of COLUMN2, which is 4.84, is larger than that of COLUMN1, and the ratio of axial force to the ultimate axial strength is also smaller than that of COLUMN1. As shown in Fig. 10(b), the proposed model slightly overestimates the ultimate resisting capacity despite its consideration of the equivalent elastic modulus of the steel. This discrepancy appears to be caused by an assumption at the post-yielding stage of a slightly larger hardening ratio of the embedded steel. However, even with this overestimation, the proposed model still effectively estimates the energy absorption capacity throughout the entire loading history and captures the pinching phenomenon. On the other hand, as shown in Fig. 10(a), a basic layered section model that does not consider the equivalent elastic modulus of steel cannot effectively estimate the energy absorption capacity, because it does not take the bond-slip effect into account.

5.2. RC frame structure subject to dynamic loading

The ability of the introduced model to describe the dynamic response of RC frame structures is assessed by comparing analytical and experimental results. The RC frame structure is specimen RCF2, which has been tested on a shaking table by Clough and Gidwani [34]. As shown in Fig. 11, this structure is a two-story, one-bay RC frame subject to a simulated strong base motion and is a 0.7 scale model of a two-story office building representative of common design and construction practice. Concrete blocks were added on every floor to take

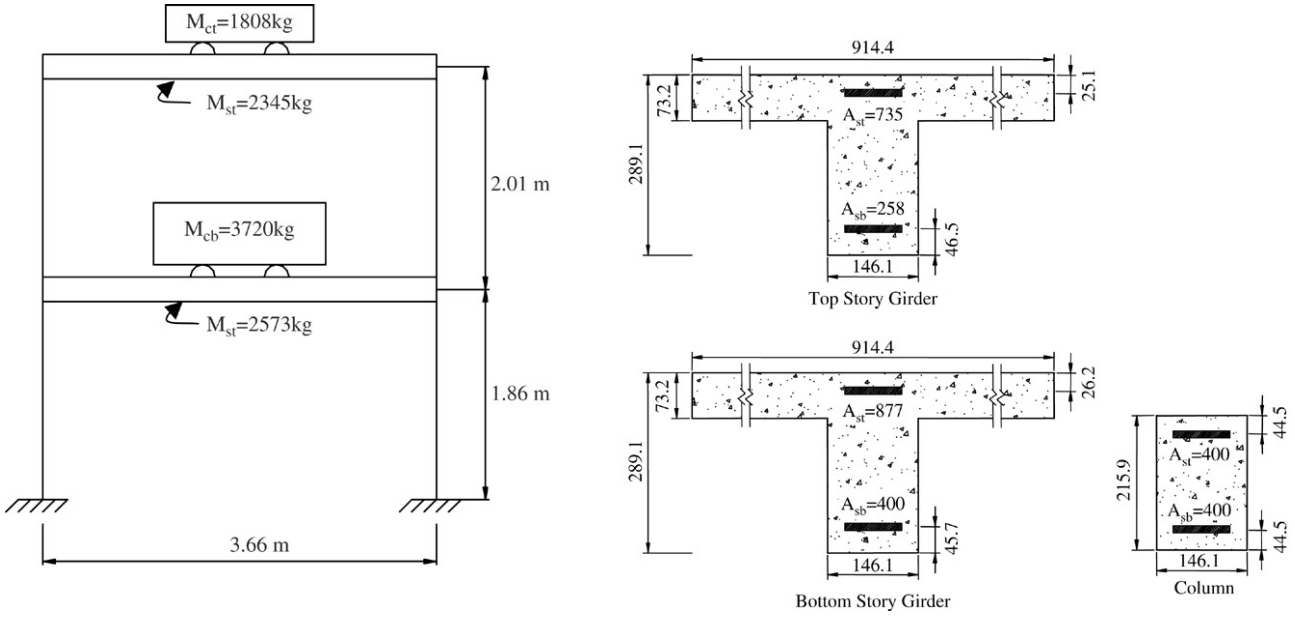

Fig. 11. Idealization of RCF2 and section geometry (unit: mm).

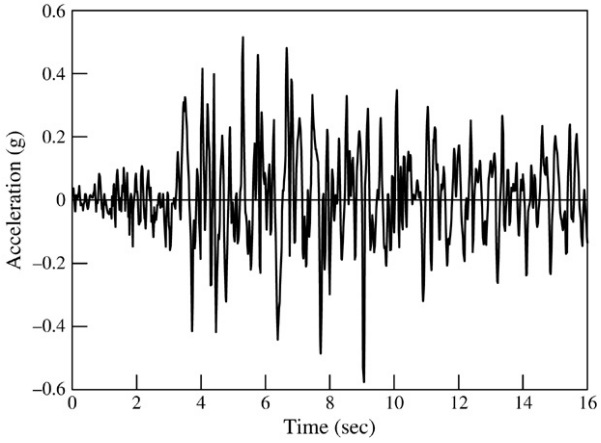

Fig. 12. N69W Taft Record W2, scaled to 0.57g.

into account the influence of the floor mass and self-weight when a base acceleration acts. The N69W Taft record from the Arvin-Tahachapi earthquake of July 1952, scaled to peak acceleration of 0.57g and referred to as W2 (see Fig. 12), was used. The same material properties of concrete and steel as those in the previous analytical study [34] are used and have the following values: $f_c' = 30$ MPa, $E_c = 2.60 \times 10^4$ MPa, $E_s = 2.0 \times 10^5$ MPa, and $f_y = 400$ MPa. The damping ratio is assumed to be 5%, which is generally used for the dynamic analysis of a RC structure. The arrangement of the shaking table and the test procedure are described in detail in Ref. [34].

Since the test results show that plastic deformations concentrate at the beam-to-column joints and/or at the column-to-foundation joints, each equivalent elastic modulus of steel, obtained from Eq. (14), is applied over the transfer length regions near each joint. The calculated values are listed in Table 3. In particular, the girders in Fig. 11, which have asymmetric T-shape sections, result in a different equivalent elastic modulus for compression steel as well as a different

Table 3
Transfer lengths and equivalent elastic modulus of steels E_{eq} for RCF2

Element	Transfer length (l_t: mm)	E_{eq} (MPa)
Top story girder	742	108,000
Bottom story girder	727	111,000
Column	647	126,000

transfer length for tension steel. However, this study uses the average values for computational convenience. According to an equation proposed by Sawyer [33], the plastic hinge length l_p is determined to be 200 mm. Therefore, the end regions of each member are modeled with an element of $l = 50$ mm, and the other regions at each member are equally idealized by using 20 elements.

The numerical results obtained on the basis of the proposed model and those from the basic layered section model are shown in Figs. 13 and 14, respectively. The results from the proposed model show very good agreement with the experimental results, indicating that the proposed model simulates the prolonged period of the structure due to stiffness degradation very well. In contrast, if the bond-slip effect is not considered, then large differences in period and displacement (approximately 16%) from the experimental data are shown (see Fig. 14). These differences are attributed to overestimation of the stiffness and the energy dissipation, which results from ignoring the bond-slip effect. The overestimated stiffness due to ignoring the bond-slip effect causes a slight phase shift at the initial loading stage and leads to a remarkable decrease in the structural displacement as the loading stage continues, as shown in Fig. 14. Comparing Fig. 13(b) with Fig. 13(c), which show the inter-story drift, the lateral deformation at the first-story column is revealed to be almost twice that of the second-story column. In addition, a comparison of Figs 13(a) and (b) with Figs 14(a) and (b) reveals that the difference of maximum

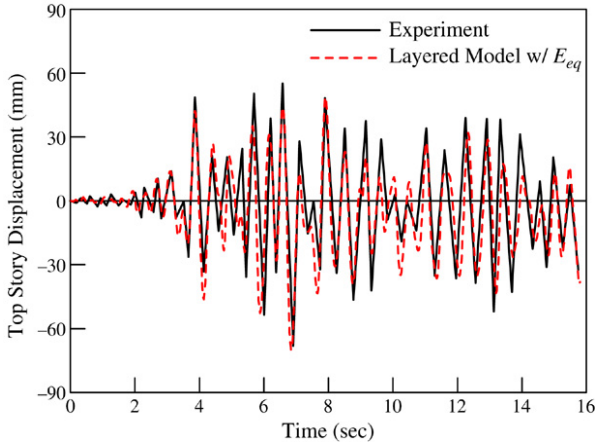

(a) Top-story displacement.

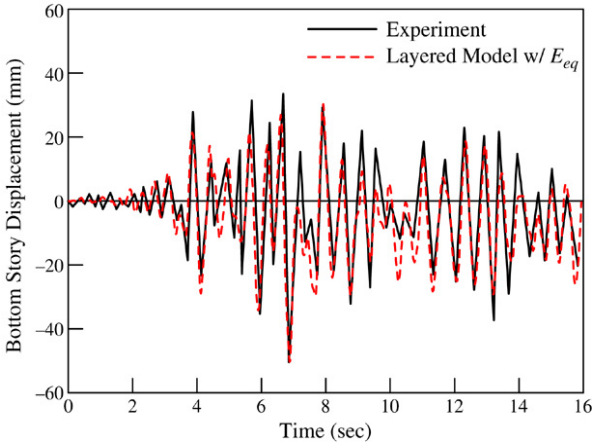

(b) Bottom-story displacement.

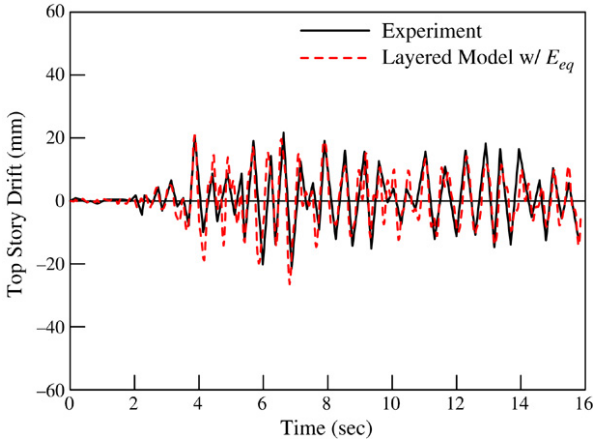

(c) Top-story drift.

Fig. 13. Displacement and drift responses from analysis with E_{eq}.

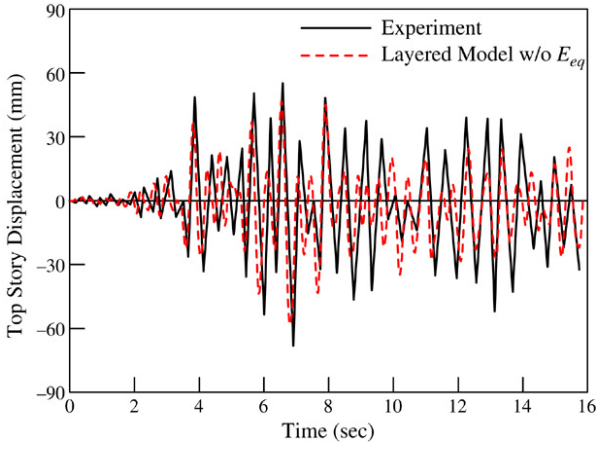

(a) Top-story displacement.

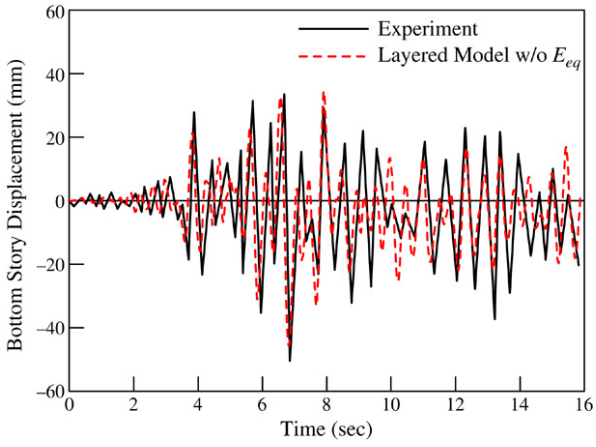

(b) Bottom-story displacement response.

Fig. 14. Displacement responses from analysis with E_s.

displacements between the two analysis procedures for E_{eq} and for E_s is approximately the same for the top and bottom story displacements. This confirms that most of the inelastic deformation of the test frame arises in the bottom story. On the other hand, the displacement–time histories in Figs 13(a) and (b) show a slight underestimation of the positive maximum displacements, as opposed to the good estimation of negative maximum displacements. This result appears to be caused by

using the average equivalent elastic modulus and transfer length in spite of the asymmetric T-shape girder, which gives different values for the compression and tension steel.

Careful investigation of the obtained numerical results in Figs. 13 and 14 yields the following three observations. First, the maximum response value for the bottom-story displacement is increased by more than 20% when the bond-slip effect is taken into account whereas the research results by Filippou et al. [1] showed a 50% increase by considering bond-slip effect. The smaller difference in this paper may be attributed to the adoption of the average stress–strain relation of steel in this paper, which indirectly considers the stress concentration of steel at cracks in an element, for application to the case ignoring bond-slip effect as well as the case considering the bond-slip effect. Second, in terms of the bond-slip effect, satisfactory agreement between experimental and analytical results is observed for the displacement time histories throughout the entire time range, although a slight discrepancy still exists in the last stage of the response time history. This discrepancy appears to be caused by the induction of gradual stiffness degradation, even at the same loading condition. Third, these figures confirm that the steel model introduced in this paper can effectively be applied to a nonlinear dynamic analysis of RC frame structures.

6. Conclusions

If the cracking behavior of RC beams is described based on a layered section approach that adopts the perfect bond assumption, it is not possible to directly consider the bond-slip effect in a layered beam model. In this regard, none of the numerical models found in the literature has taken the bond-slip effect into account. In an effort to solve this problem, this paper introduces a stress–strain relation of reinforcing steel designed through indirect consideration of the bond-slip effect between the reinforcing steel and its surrounding concrete. The introduced stress–strain relation of steel is also recommended for use in the maximum moment regions bounded by the transfer length, because the bond-slip accompanying the cracking behavior is usually concentrated in these regions.

Correlation studies of the proposed model with experimental results from two typical RC beams and a two-story one-bay RC frame verify that the proposed model is capable of describing the cyclic behavior of RC beams as well as the dynamic response of RC frame structures with satisfactory accuracy. The analytical studies demonstrate that considering the bond-slip effect improves the accuracy of the numerical results and is essential in the cyclic and dynamic analysis of RC structures. In contrast, ignoring the bond-slip effect leads to overestimation of the energy absorption capacity and the stiffness of the structure during cyclic excitation. That is, the fundamental period and the displacement response of the structure are underestimated. Therefore, in order to predict the cyclic and dynamic structural behaviors of RC beams and beam-to-column subassemblages, the bond-slip effect must be taken into account. The introduced numerical model makes it possible to consider the bond-slip effect in a layered RC beam element.

Acknowledgment

The authors would like to thank the Infra-Structures Assessment Research Center (ISARC) funded by Korea Ministry of Construction and Transportation (MOCT) for financial support.

References

[1] D'Ambrisi A, Filippou FC. Correlation studies on an RC frame shaking-table specimen. Earthquake Engineering and Structural Dynamics 1997; 26:1021–40.
[2] Kwak HG, Kim SP, Kim JE. Nonlinear dynamic analysis of RC frames using cyclic moment–curvature. Structural Engineering and Mechanics 2004;17(3–4):357–78.
[3] Roufaiel MSL, Meyer C. Analytical modeling of hysteretic behavior of RC frames. Journal of Structural Engineering 1987;113(3):429–44.
[4] Takeda T, Sozen MA, Nielsen NN. Reinforced concrete response to simulated earthquake. Journal of the Structural Division ASCE 1970; 96(ST-12):2557–73.
[5] Kwak HG, Kim SP. Cyclic moment–curvature relation of an RC beam. Magazines of Concrete Research 2002;54(6):435–47.
[6] Taucer T, Spacone E, Filippou FC. A fiber beam-column element for seismic response analysis of reinforced concrete structures, Earthquake Engrg. Research Center Report No. EERC 91-17. Berkeley (CA): Univ. of California; 1991.
[7] Clough RW, Johnson SB. Effect of stiffness degradation on earthquake ductility requirements. In: Proceedings of Japan Earthquake Engineering symposium. 1966.
[8] Chung YS, Meyer C, Shinozuka M. Modeling of concrete damage. ACI Structural Journal 1998;86(3):259–71.
[9] Dowell RK, Seible F, Wilson EL. Pivot hysteresis model for reinforced concrete members. ACI Structural Journal 1998;95(5):607–17.
[10] Assa B, Nishiyama M. Prediction of load–displacement curve of high-strength concrete columns under simulated seismic loading. ACI Structural Journal 1998;95(5):547–57.
[11] Watson S, Park R. Simulated seismic load tests on reinforced concrete column. Journal of Structural Engineering 1994;120(6):1825–49.
[12] Kwak HG, Kim JK. Ultimate resisting capacity of slender RC columns. Computers Structures 2004;82:901–15.
[13] Park R, Kent DC, Sampton RA. Reinforced concrete members with cyclic loading. Journal of the Structural Division ASCE 1972;98(7):1341–60.
[14] Scott BD, Park R, Priestley MJN. Stress-strain behavior of concrete confined by overlapping hoops at low and high strain rates. ACI 1982; 79(1):13–27.
[15] Kwak HG, Filippou FC. Finite element analysis of reinforced concrete structures under monotonic loabelds. Report no. UCB/SEMM-90/14. Berkeley (CA): Univ. of California; 1990.
[16] Welch GB, Haisman B. Fracture toughness measurements of concrete. Report no. R42. Sydney: Univ. of New South Wales; 1969.
[17] Comite Euro-International du Beton, RC elements under cyclic loading: state of the art report. London: Thomas Telford Services Ltd.; 1996.
[18] Mansour M, Lee JY, Hsu TTC. Cyclic stress–strain curves of concrete and steel bars in membrane elements. Journal of Structural Engineering 2001;127:1402–11.
[19] Karsan ID, Jirsa JO. Behavior of concrete under compressive loading. Journal of the Structural Division 1969;95.
[20] Vecchio FJ. Towards cyclic load modeling of reinforced concrete. ACI Structural Journal 1999;96:193–202.
[21] Stevens NJ, Uzumeri SM, Collins MP, Will GT. Constitutive model for reinforced concrete finite element analysis. ACI Structural Journal 1991; 88(1):49–59.
[22] Belarbi A, Hsu TTC. Constitutive laws of concrete in tension and reinforcing bars stiffened by concrete. ACI Structural Journal 1994;91(4): 465–74.

[23] Gergely P, Lutz LA. Maximum crack width in reinforced concrete flexural member. Causes, mechanism, and control of cracking in concrete (SP-20). Detroit: American Concrete Institute; 1968. p. 87–117.
[24] Somayaji S, Shah SP. Bond stress versus slip relationship and cracking response of tension members. ACI Journal 1981;78(3):217–25.
[25] Mirza SM, Houde J. Study of bond stress–slip relationships in reinforce concrete. ACI Journal 1979;76(1):19–45.
[26] Menegotto M, Pinto PE. Method of analysis for cyclically loaded reinforced concrete plane frame including changes in geometry and nonelastic behavior of elements under combined normal force and bending. In: Proceedings, IABSE symposium on resistance and ultimate deformability of structures acted on by well defined repeated loads. Lisbon; 1973.
[27] Pinto PE, Giuffre A. Comportamento del cemento armato per sollecitazioni cicliche di forte intensita. Giornale del Genio Civile 1970;5.
[28] Filippou FC, Popov EP, Bertero VV. Effects of bond deterioration on hysteretic behavior of reinforced concrete joints. Earthquake engineering research center, report UCB/EERC-83/19. Berkeley (CA): University of California; 1983.
[29] Kwak HG, Seo YJ. Long-term behavior of composite girder bridges. Computers Structures 2000;74(5):583–99.
[30] Low SS, Moehle JP. Experimental study of reinforced concrete columns subjected to multi-axial cyclic loading. Earthquake engineering research center, report no. EERC 87/14. Berkeley (CA): Univ. of California; 1987.
[31] Chopra AK. Dynamics of Structures. Englewood Cliffs (NJ): Prentice-Hall; 1995.
[32] Wight JK, Sozen MA. Strength decay of RC columns under shear reversals. Journal of the Structural Division 1975;101(ST5):1053–65.
[33] Sawyer HA. Design of concrete frames for two failure states. In: Proceedings of the international symposium on the flexural mechanics of reinforced concrete, ASCE-ACI; 1964. p. 405–31.
[34] Clough RW, Gidwani J. Reinforced concrete frame 2: seismic testing and analytical correlation. Earthquake engineering research center report no. EERC 76-15. Berkeley (CA): Univ. of California; 1976.